IOPscience iopscience.iop.org

Home Search Collections Journals About Contact us My IOPscience

The influence of microcrystalline inhomogeneities embedded in amorphous In_xSe_{100-x} films on their electrical and optical properties

This article has been downloaded from IOPscience. Please scroll down to see the full text article.

1996 J. Phys.: Condens. Matter 8 3439

(http://iopscience.iop.org/0953-8984/8/19/019)

View the table of contents for this issue, or go to the journal homepage for more

Download details:
IP Address: 171.66.16.208
The article was downloaded on 13/05/2010 at 16:38

Please note that terms and conditions apply.

J. Phys.: Condens. Matter **8** (1996) 3439–3451. Printed in the UK

The influence of microcrystalline inhomogeneities embedded in amorphous In_xSe_{100-x} films on their electrical and optical properties

J C Bernède†, S Marsillac†, A Conan† and A Godoy‡

† Université de Nantes, LPME, Faculté des Sciences et des Techniques, 2 rue de la Houssinière, 44072 Nantes Cédex 03, France

‡ Laboratorio de Polimeros, Facultad de Quimica, Prontifica Universidad Catolica de Chile, PO Box 6177, Santiago, Chile

Received 25 October 1995, in final form 5 February 1996

Abstract. In the past, In_xSe_{100-x} amorphous layers have been described as n or p type according to their majority carriers. The majority carrier type varies from one study to another, even with films of the same composition, which is a very serious problem. In this paper we explain this discrepancy by demonstrating that microcrystallite inhomogeneities are present in the amorphous In_xSe_{100-x}. While x-ray diffraction patterns are typical of amorphous samples, the selected-area diffraction obtained using a transmission electron microscope depends on the area studied. It is shown that the layers are constituted of microcrystallites embedded in an amorphous matrix. Therefore the majority carrier type changes when the p-type nature of the amorphous matrix is masked by the n-type nature of the crystallites at the percolation threshold. Of course this percolation threshold depends not only on the composition of the layer but also on the deposition process, which explains the different majority carrier types found for identical composition. The two critical temperatures measured from the conductivity curves can be attributed to the phase transition α-$In_2Se_3 \rightarrow \beta$-$In_2Se_3$ of the microcrystallites (the first one) and the overall crystallization of the layer (the second one). The typical optical absorption and differential thermal analysis properties are explained in the same way.

1. Introduction

InSe compounds have been a subject of interest and of controversy because of their ability to be n or p type. Some papers insist that n-type amorphous films [1–3] have been obtained in the InSe system and some say that they have not [4–6].

Usual amorphous chalcogenides are well known to be p type [7, 8]. However, one system among the chalcogenide compounds that have been studied is well known to exhibit n-type behaviour; it is the system Ge–Bi–Se [9–11]. The system Ge–Bi–Se is the first example known to show n-type conduction in chalcogenide glasses. However, if there is still some difference as regards the explanation of the appearance of the n-type conduction, all researchers have reported the same experimental results concerning the conduction type. In contrast to this case, in the InSe system the experimental results themselves are different from paper to paper, as mentioned above, even for films of the same composition. This discrepancy in the experimental results is a very serious problem which should be solved. If it is possible to explain why n-type conduction is obtained for some composition and experimental conditions, it will be easier to resolve the discrepancy in the experimental results.

0953-8984/96/193439+13$19.50 © 1996 IOP Publishing Ltd

In an earlier paper [12] we suggested that amorphous In_xSe_{100-x} is probably, like the other chalcogenides, p type and that the change of carrier type should be attributed to the presence of small crystallites in the layers. In_2Se_3, InSe and In_4Se_3 stoichiometric crystals are well known to be n type [13–17], and therefore we have proposed that the change of carrier sign (p $\rightarrow$ n) when the In percentage increases should be attributed to the percolation threshold between these crystallites.

In this paper, we report the results of new experimental measurements such as those of optical absorption, conductivity variation with the temperature and differential thermal analysis (DTA) that have been performed. The typical compositions of the In_xSe_{100-x} films studied are: $x = 40$, $x = 50$ and $x = 60$. All of the films studied have been checked by scanning and transmission electron microscopies (SEM and TEM), microprobe analysis, x-ray photoelectron spectroscopy (XPS) and x-ray diffraction.

All of the experimental results can be explained by the presence of microcrystallite inhomogeneities in the amorphous In_xSe_{100-x} films, and are in accordance with the percolation threshold hypothesis for explaining the carrier type change.

2. Experimental techniques

The starting material was prepared by mixing quantities of high-purity (99.999%) indium and selenium pellets in various calculated ratios. The mixture was sealed in an evacuated Pyrex tube and heated at 823 K for 24 hours. In_xSe_{100-x} thin films were obtained by classical thermal evaporation of the powder from a molybdenum boat, under a vacuum better than 10^{-4} Pa. A shutter was used at the beginning and at the end of the heating of the boat, to avoid contamination of the substrate. The evaporation boat has a special configuration (two superposed multiholed covers) in order to avoid the calefaction of the In_xSe_{100-x} powder. The substrates were of glass, NaCl freshly cleaved crystal for TEM measurement or stainless-steel slides for XPS analysis. The evaporation rates (1 to 1.5 nm s^{-1}) and the film thicknesses were measured *in situ* by the vibrating-quartz-crystal method. The thickness was also checked with a mechanical stylus, in order to estimate the surface roughness of the thin films.

The structure of the films was checked by x-ray diffraction. The morphology of the films was obtained visually by SEM.

The crystallographic state of the films was checked by TEM. In order to prepare the layers for TEM analysis, the NaCl crystals were dissolved in distilled water and the films were picked up with the usual copper grids. The TEM images were obtained using a 'JEM 100 CX' electron microscope at a '100 kV acceleration voltage'. XPS analyses were performed with a magnesium x-ray source (1253.6 eV) operating at 10 kV and 10 mA. XPS measurements were carried out at Nantes (University of Nantes—CNRS). The energy resolution was 1 eV at a pass energy of 50 eV. High-resolution scans with a good signal-to-noise ratio were obtained in the Se 3d and In 3d regions of the spectrum. The quantitative studies were based on the determination of the Se 3d and In $3d_{5/2}$ peak areas with 0.57 and 3.8, respectively, as sensitivity factors (the sensitivity factors of the spectrometer are given by the manufacturer, Leybold). The oxygen pollution at depth was studied by recording successive XPS spectra obtained after argon-ion etching for short periods. Sputtering was accomplished at pressures of less than 5×10^{-4} Pa, with a 10 mA emission current and 5 kV beam energy using an ion gun. The Ar^+-ion beam was scanned over the entire sample surface. Quantitative analysis was also achieved by electron microprobe analysis.

The optical measurements were carried out at room temperature using a CARY spectrophotometer. The optical density (OD) was measured at wavelengths from 2 to

0.4 μm. The absorption coefficient α was calculated as described earlier [12] from the measured transmission of two films obtained in the same experimental conditions but with small thickness differences.

For the electrical measurements gold electrodes were evaporated after the deposition of the In_xSe_{100-x} layers. The gold was selected because gold thin films gave a good ohmic contact. Copper wires were attached to the gold using gold or silver paste. The dc conductance was measured by a conventional method with an electrometer between 300 and 625 K. When this electrometer was used to measure resistance (ohm function), the currents generated during measurements by the electrometer used were between 100 mA ($R = 2$ kW) and 1 nA ($R = 20$ GW). Electrical measurements were carried out in the dark.

The signs of the carriers were checked by the hot-probe technique.

We also proceeded to differential thermal analysis (DTA). The apparatus used for DTA was a Perkin–Elmer DSC 1B. Measurements were made and the instruments calibrated at a scan rate of 10 K min^{-1}.

3. Experimental results

The thickness of the films ranged from 100 to 700 nm. It turns out that the thickness variations did not notably affect the experimental results, except the optical gap measurements for which films around 500 nm thick were systematically used. In any case, for each measurement, results are reported for films of the same thickness.

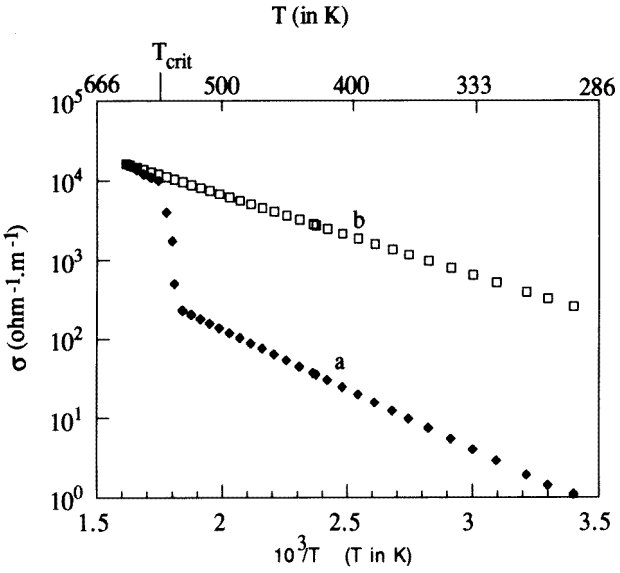

Figure 1. Typical $\ln(\sigma)$ versus $1/T$ results for $In_{60}Se_{40}$ layers. (a) The first measurement. (b) The second measurement.

3.1. Conductivity measurements

The experimental results for the dark conductivity and its variation in the case of $In_{60}Se_{40}$ and $In_{40}Se_{60}$ amorphous films are shown in figures 1 and 2, 3 respectively. The results

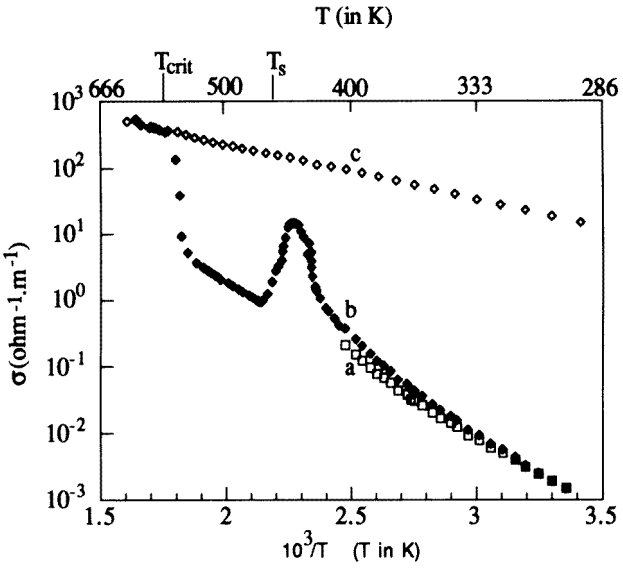

Figure 2. Typical $\ln(\sigma)$ versus $1/T$ results for $In_{40}Se_{60}$ layers. (a) The first measurement ($T < T_s$). (b) The second measurement. (c) The third measurement.

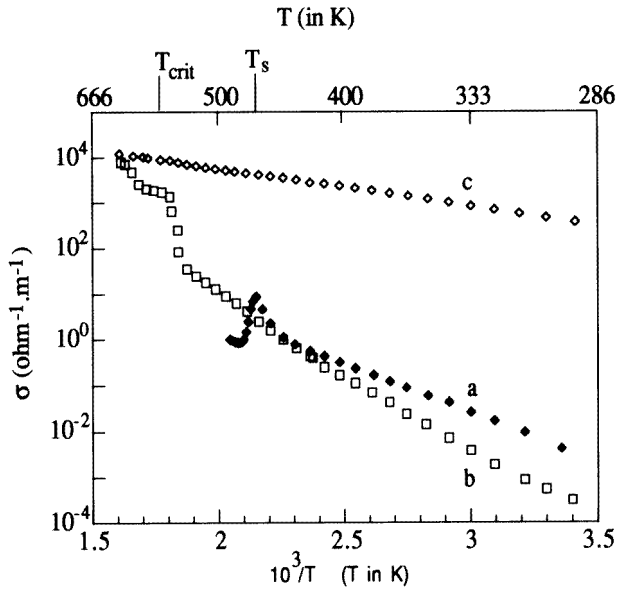

Figure 3. Typical $\ln(\sigma)$ versus $1/T$ results for $In_{40}Se_{60}$ layers. (a) The first measurement ($T_s < T < T_{crit}$). (b) The second measurement. (c) The third measurement.

obtained with $In_{50}Se_{50}$ layers are not represented since the shape of the curves is the same as that obtained with $In_{40}Se_{60}$. It can be seen that in the case of $In_{60}Se_{40}$ layers there is an irreversible conductivity increase for a critical temperature labelled T_{crit} (figure 1). In the case of $In_{40}Se_{60}$ and $In_{50}Se_{50}$ layers, if this critical temperature is still present, there is

Table 1. The evolution of the carrier type and of the optical gap of the layer with composition (b: before T_s is reached; a: after T_s is reached).

Sample	$In_{40}Se_{60}$		$In_{50}Se_{50}$		$In_{60}Se_{40}$	
Carrier type	p		p		n	
Composition (at.%)	Se	In	Se	In	Se	In
Microprobe analysis	40	60	50	50	58	42
XPS analysis	40	60	49	51	57	43
Optical gap	b: 1.4	a: 1.6	b: 1.1	a: 1.3	0.8	

another singular temperature smaller than T_{crit}. We have labelled this temperature T_s. It can be seen that just before this temperature is reached there is a quite fast increase of the conductivity and for $T > T_s$ there is a fast decrease of the conductivity (figure 2). It can be seen in figure 3 that the phenomenon corresponding to T_s is also irreversible, while when $T < T_s$ the measurements are reproducible (figure 2, curves a and b). Moreover it can be seen in figure 3 that at room temperature, when equilibrium is reached (after several hours), the conductivity of the sample is at least one order of magnitude smaller after the heating with T in the range $T_s < T < T_{crit}$ than before.

Therefore the properties of the films have been systematically studied in the different conductivity domains: (1) $T < T_s$; (2) $T_s < T < T_{crit}$; (3) $T > T_{crit}$, and the results are given in the section below.

3.2. Other thin-film characterizations

The changes of the carrier type with composition are given in table 1. It can be seen that the films which are usually p type become n type for high In atomic concentration.

The surface of the layers has been investigated visually by scanning electron microscopy. The morphology of the surfaces of all of the layers, of whatever composition, is smooth without any features as is usual in the case of amorphous layers. The composition has been measured by microprobe analysis; this technique has also been used to check the homogeneity of the layers. The results are given in table 1. It can be seen that, in the experimental uncertainty range of the apparatus, the composition of the layers is the same as that of the initial powder. Also the variation from one point to another never exceeds 2 at.% which corresponds to the precision of the apparatus. If the surface microphotographs of the layers are identical whatever their compositions are, in the composition range investigated in this work, no more information can be obtained from XRD since all of the spectra are flat (figure 4(*a*)), whatever the compositions of the layers are, which means that 'macroscopically' the films are amorphous. The same XRD spectra are obtained after the heating with temperature T in the range $T_s < T < T_{crit}$ (figure 4(*b*)). But it should be noted that above T_{crit} the XRD spectra show that the films are crystallized (figure 4(*c*)).

The results appear to be quite different when a transmission electron microscope is used as the investigating apparatus. The results (transmission electron micrographs and electron diffraction patterns) obtained with the different kinds of sample are reported in figures 5 to 7. It can be seen that whatever the layer is, there are systematic inhomogeneities visible in the electron micrographs. However, while the inhomogeneity densities of the $In_{40}Se_{60}$ samples before T_s is reached (figure 5(*a*)) or after T_s is reached (figure 6(*a*)) are not very different, it is far higher in the case of $In_{60}Se_{40}$ (figure 7(*a*)). Moreover, while the electron diffraction patterns obtained from the smooth clear matrix of the layers (region 1 of each

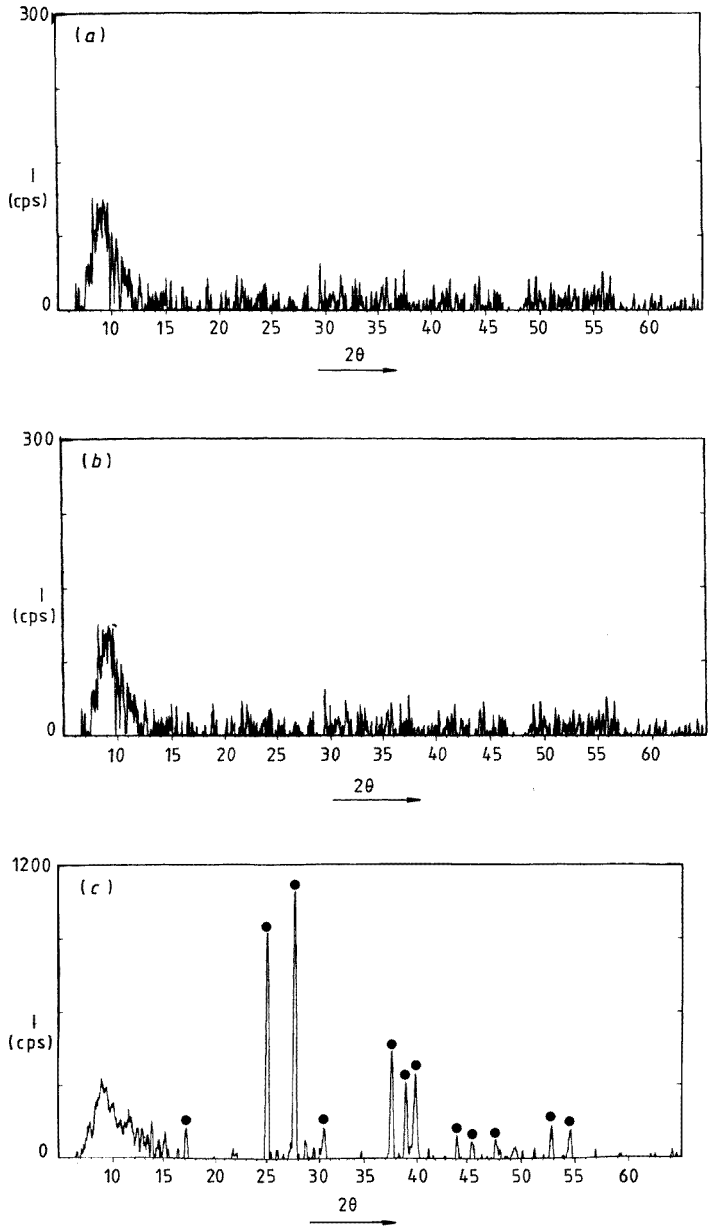

Figure 4. XRD spectra of an $In_{40}Se_{60}$ layer: (*a*) after deposition; (*b*) after heating with T in the range $T_s < T < T_{crit}$; and (*c*) after heating with $T > T_{crit}$ (●: In_2Se_3 peaks). The large peak on the small-angle side corresponds to the amorphous glass substrate.

film (figures 5(*b*), 6(*b*), 7(*b*))) are typical of an amorphous sample, those obtained from the small dark inhomogeneities (region 2 of each film (figure 5(*c*), 6(*c*), 7(*c*))) are typical of small and randomly oriented microcrystallites.

We have also proceeded to optical measurements on the different samples. The absorption coefficient α has been calculated for two samples with different thicknesses.

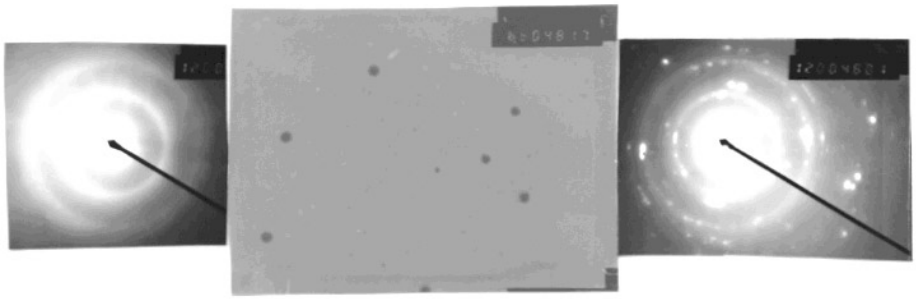

(*b*) (*a*) (*c*)

Figure 5. (*a*) A transmission electron micrograph of an $In_{40}Se_{60}$ film before heating; and (*b*) and (*c*) electron diffraction patterns of regions 1 and 2 (see the text) in the micrograph respectively.

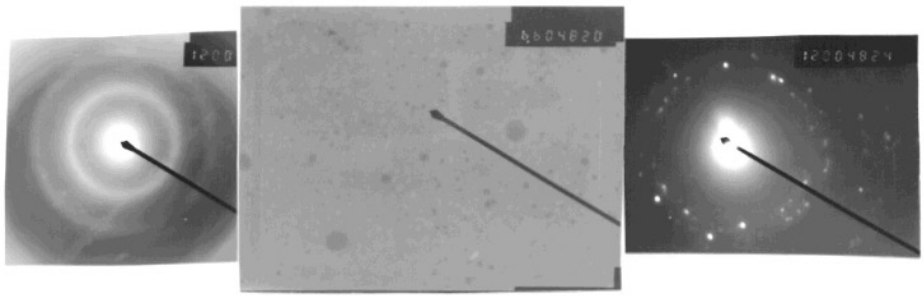

(*b*) (*a*) (*c*)

Figure 6. (*a*) A transmission electron micrograph of an $In_{40}Se_{60}$ film after heating with T in the range $T_s < T < T_{crit}$; and (*b*) and (*c*) electron diffraction patterns of regions 1 and 2 (see the text) in the micrograph respectively.

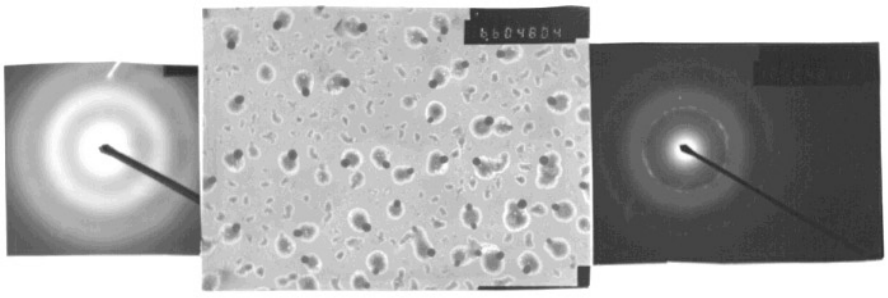

(*b*) (*a*) (*c*)

Figure 7. (*a*) A transmission electron micrograph of an $In_{60}Se_{40}$ film before heating; and (*b*) and (*c*) electron diffraction patterns of regions 1 and 2 (dark inhomogeneities) in the micrograph respectively.

It has been shown already that the band gap of amorphous In_xSe_{100-x} layers varies with the thickness [18–20]; therefore we have used samples with small thickness differences in order to minimize this variation. The optical band gap of the In_xSe_{100-x} has been estimated by extrapolating the plots of $\alpha h\nu = A(h\nu - E_g)^n$ to zero absorption (figure 8). The value

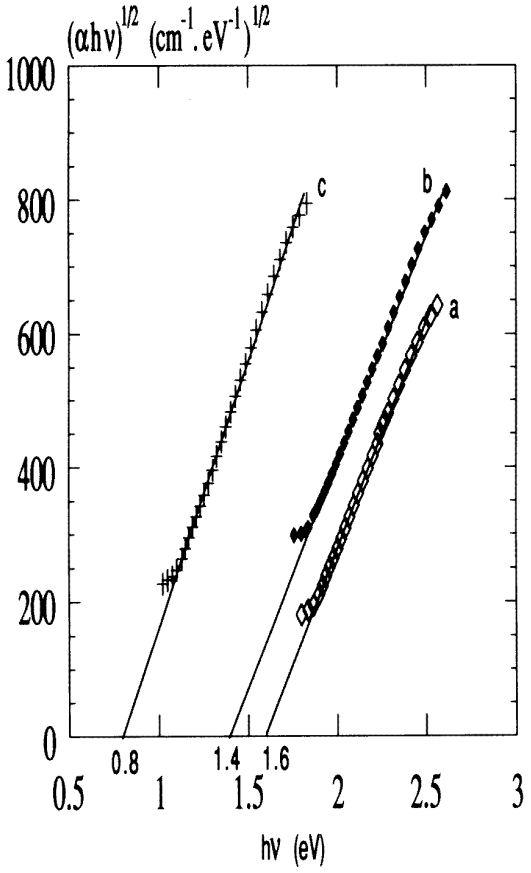

Figure 8. The variation in optical absorption $(\alpha h\nu)^{1/2}$ with the photon energy $h\nu$ for: (a) $In_{40}Se_{60}$ layers after heating with T in the range $T_s < T < T_{crit}$; (b) $In_{40}Se_{60}$ layers before heating; and (c) $In_{60}Se_{40}$ layers.

of n has been taken equal to two as proposed by Mott and Davis [8]. The results obtained are summarized in table 1. It can be seen that, as expected, the band gap increases with the number of at.% of Se but also when the p-type samples are heated with the temperature in the range $T_s < T < T_{crit}$.

The averaged composition and purity of the layers have been checked by XPS analysis. It can be seen in table 1 that the surface composition is not different from that of the bulk composition measured by microprobe analysis. After an etching of one minute the C 1s and O 1s peaks have nearly disappeared, which confirms the purity of the layers.

Finally, the differential thermal analysis is reported in figure 9. It can be seen that two exothermic peaks are evident during the first heating of the sample (curve (*a*)). One narrow peak appears at a temperature $T = T_{crit}$ measured from the conductivity curves, while another broad one appears at a temperature near the temperature $T = T_s$. A first heating cycle limited to temperatures in the range $T_s < T < T_{crit}$ exhibits a peak at $T \approx T_s$ (curve (*b*)). During a second heating cycle up to $T = 673$ K, this peak has disappeared and only the narrow peak appears at $T \approx T_{crit}$ (curve (*c*)).

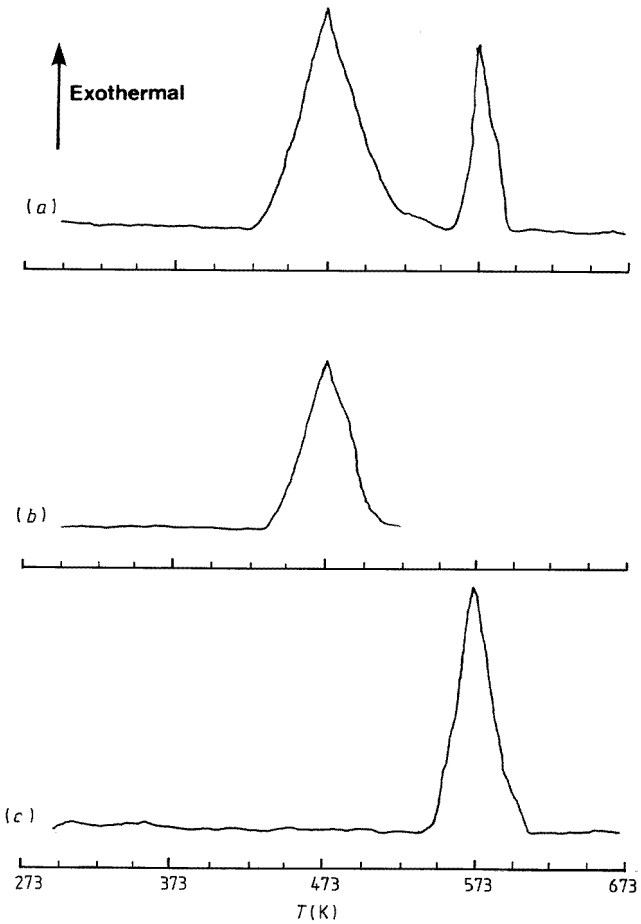

Figure 9. Typical differential thermal analysis of an $In_{40}Se_{60}$ layer. (*a*) The heating cycle up to $T = 673$ K (sample 1). (*b*) The first heating cycle with the temperature in the range $T_s < T < T_{crit}$ (sample 2). (*c*) The second heating cycle up to $T = 673$ K (sample 2).

4. Discussion

While the films appear to be roughly homogeneous (from XRD and SEM) it has been shown by TEM that the In_xSe_{100-x} films contain a lot of microscopic microcrystallites. Moreover the density of microcrystallites increases with the In at.% content of the layers (figures 5(*a*), 6(*a*), 7(*a*)). These microscopic heterogeneities significantly affect the electrical properties of the samples [21]. Statistical EMA (effective-medium approximation) models (Maxwell-Garnett [21], Bruggeman [21], ...) have been used to give an account of the experimental results. The Bruggeman approach shows that the percolation threshold between low and high conductivity is achieved for a minimum amount of conductor of about 30%. However, this model supposes spherical regions randomly distributed in the insulating matrix. In fact a filamentary percolation threshold is more probable and experimental results have shown that in that case 15% to 20% are sufficient. Such a model has been proposed by Tichy *et al* in the case of $In_{50}Se_{50}$ samples [11]. Moreover Hogg *et al* [22] has shown that, in the In_xSe_{100-x} system, In tends to segregate when it is added in too large quantities.

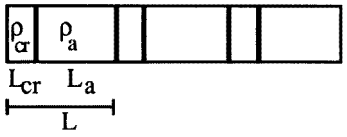

Figure 10. Scheme 1.

Therefore we propose that in the case of $In_{60}Se_{40}$, since the density of microcrystallites is high, the percolation threshold has been reached, which explains the n-type behaviour of these layers since the In_xSe_{100-x} crystals are n type. For $T \geqslant T_{crit}$ the overall amorphous matrix crystallizes and the conductivity increases strongly. In the cases of $In_{40}Se_{60}$ and $In_{50}Se_{50}$ the densities of the microcrystallites are far smaller; therefore we are below the percolation threshold. In that case, resistivity and thermoelectric power can be roughly described in a one-dimensional model by

$$R = \sum (R_1 + R_2) \rightarrow \rho = \rho_a \left(1 - \frac{L_{cr}}{L}\right) + \rho_{cr} \left(\frac{L_{cr}}{L}\right) \tag{1}$$

where the subscript 'a' is used for amorphous and 'cr' for crystalline; R is the resistance, ρ the resistivity and L the length; and by

$$S = \frac{\rho_a(1 - L_{cr}/L)S_a + \rho_{cr}(L_{cr}/L)S_{cr}}{\rho_a(1 - L_{cr}/L) + \rho_{cr}(L_{cr}/L)} \tag{2}$$

where S is the thermoelectric power. Usually

$10^2 < \rho_a\ (\Omega\ \mathrm{m}) < 10^4$	[2, 4, 19, 23, 24]
$S_a = 500\ \mu\mathrm{V\ K^{-1}}$	[4]
$3 \times 10^{-2} < \rho_{cr}\ (\Omega\ \mathrm{m}) < 10^{-1}$	[14, 25]
$S_{cr} = 20\ \mu\mathrm{V\ K^{-1}}$	[26]

while statistically (figures 5(*a*) and 7(*a*))

$$\frac{1}{25} < \frac{L_{cr}}{L} < \frac{1}{10}.$$

This is shown schematically in figure 10.

Since $S_{cr} \ll S_a$, $\rho_{cr} \ll \rho_a$ and $L_{cr} \ll L$, S_a will be the most important term of S in (2) and the sign of S will be the sign of S_a—that is to say, below the percolation threshold, the carrier type measured will be the p type.

Of course the percolation threshold, that is to say the density of microcrystallites, depends on the In concentration but also on the experimental conditions, such as the deposition technique (the size of the evaporation crucible, the temperature of the crucible, the deposition rate, the dynamic vacuum during evaporation, the substrate cleanliness, the substrate temperature, ...). Therefore it is easy to see that the percolation threshold will be different from one deposition to another one, even for layers with the same composition.

Therefore the percolation theory is able to explain easily the different carrier types obtained from paper to paper.

However, if the discrepancy in the experimental results is well understood by using the percolation threshold model, the conductivity results obtained for the layer below this percolation threshold (figures 2 and 3) are still to be explained.

First of all, as shown by XRD (figure 4(*c*)) the irreversible conductivity change above T_{crit} can be attributed to the layer crystallization. This result is corroborated by DTA results

since the narrow exothermic peak situated at the same temperature has the typical shape of a crystallization peak.

Table 2. Lattice parameters deduced from selected-area diffraction (SAD) patterns (figures 5(*c*), 6(*c*), 7(*c*)).

$d(hk\ell)$ (10^{-1} nm)		4.157	3.425	3.420	3.340	2.814	2.579	2.149	2.155	2.078	1.813
Planar attribution ($hk\ell$)	α-In_2Se_3		101			104		107			109
	β-In_2Se_3			101			105		107		
	InSe	006			012					0012	
$d(hk\ell)$ (10^{-1} nm)	$In_{40}Se_{60}$ before heating		3.43			2.82		2.14			1.80
	$In_{40}Se_{60}$ after heating for $T_s < T < T_{crit}$			3.42			2.58		2.16		
	$In_{60}Se_{40}$ before heating	4.15			3.32					2.06	

On the other hand, the $In_{40}Se_{60}$ films heated with the temperature kept in the range $T_s < T < T_{crit}$ are still amorphous (figures 4(*b*) and 6(*b*)). However, if the electron diffraction patterns of the amorphous matrix before and after heating with T kept in the range $T_s < T < T_{crit}$ are identical, this is not the case for the electron diffraction patterns of the microcrystallites. It can be effectively seen in figures 5(*c*) and 6(*c*) that the electron diffraction patterns of the microcrystallites are not the same. More accurately, it can be seen in table 2 that, before annealing the $In_{40}Se_{60}$ layers, the patterns of the crystallites can be attributed to the α-In_2Se_3 phase, while after heating between T_s and T_{crit} they can be attributed to the β-In_2Se_3 phase. The lattice parameters of the two phases are not very different, and other characterizations are necessary to confirm this attribution. DTA and conductivity measurements can be used for this purpose.

The second DTA peak is situated at around $T = 476$ K which is the temperature at which the singular conductivity feature intervenes; therefore we can imagine that those two phenomena are similar. Since these phenomena cannot be attributed to the crystallization of the layer, the shape of the DTA peak shows that they should be attributed to a phase modification. Selected-area diffraction (SAD) of the amorphous matrix shows that the amorphous phase stays the same and therefore the phase change intervenes in the microcrystallites. It is well known that hexagonal In_2Se_3 exhibits many phases such as α-In_2Se_3 and β-In_2Se_3, with

$$\alpha\text{-}In_2Se_3 \overset{T\approx 473\ \mathrm{K}}{\longrightarrow} \beta\text{-}In_2Se_3 \qquad [27\text{–}29].$$

By comparison with our measurements, similar evaluations of the conductivity and the temperature have been obtained by other authors for polycrystalline InSe powders. They have attributed the critical temperature to the transition at $T = 473$ K $\approx T_s$ from the α-phase to the β-phase [14, 30–32]. As shown by equation (1), the resistivity of the sample depends not only on the conductivity of the amorphous phase but can also partly depend on the conductivity of the crystallites. Therefore we can imagine that before T_s is reached the conductivity increases more and more quickly when the temperature increases, as is usual in the case of polycrystalline semiconductor films, which explains the bending of the curve of $\ln(\sigma)$ versus $10^3/T$ when T increases [33]. When $T = T_s$ there is a transition from the α- to the β-In_2Se_3 phase. As the conductivity of this β-phase is two orders of

magnitude smaller than that of the α-phase, there is a fast decrease of the conductivity and then the conductivity increases again as temperature increases up to $T = T_{crit}$. The smaller conductivity of the β-phase can also explain the decrease of the room temperature conductivity of the layers after a heating with the temperature in the range $T_s < T < T_{crit}$ (figure 3).

While it is known that the $\alpha \rightarrow \beta$ transition is reversible, it can be seen in figure 3 that the phenomenon occurring at $T = T_s$ is irreversible. This irreversibility is corroborated by the curves (*b*) and (*c*) of figure 9. However, it has been shown that if the $\alpha \rightarrow \beta$ transition is reversible in the case of a bulk sample, this is not true in the case of thin films [30, 31]. After the $\alpha \rightarrow \beta$ transition, films kept this new configuration even when the temperature decreased to room temperature. Moreover Eddrief [30] has shown that the transition temperature decreases when the indium content in the films increases. He has also shown that when the substrates are heated, the films are directly stabilized in the β-phase. It is well known that during thin-film deposition the substrate temperature T_{sub} increases progressively; therefore we can imagine that the indium content of $In_{60}Se_{40}$ is high enough to decrease the phase transition temperature $T(\alpha \rightarrow \beta)$ sufficiently that in places $T(\alpha \rightarrow \beta) < T_{sub}$; this may explain why the microcrystallites which appear are in the β-phase, which justifies T_s not being present in figure 1, curve a.

In the above discussion it is supposed that in the formula (1) $\rho_{cr}(L_{cr}/L)$ is not inconsiderable compared to $\rho_a(1 - L_{cr}/L)$. The small increase of the optical gap after heating with $T > T_s$ (figure 8 and table 1) can be explained in the same way. In a heterogeneous system, assume that the sample can be divided into two phases, and let N_{cr} and N_a be the densities of the crystalline and the amorphous regions in the bulk of the layer. α, the absorption coefficient, is assumed to be given by [34]

$$\alpha = \frac{\alpha_{cr} N_{cr} + \alpha_a N_a}{N_{cr} + N_a}$$

where α_{cr} and α_a are absorption coefficients of the crystalline and amorphous states. From this equation, α will depend on the absorption coefficient of the crystalline phase and therefore of its optical gap. Since the optical gap of the β-In_2Se_3 phase is greater than that of the α-In_2Se_3 phase, the measured optical gap will increase when α-In_2Se_3 gives way to β-In_2Se_3—that is to say when $T > T_s$.

5. Conclusion

The change of conductivity type with In content of the In_xSe_{100-x} amorphous layers is related to the crystallite inhomogeneities systematically present in these layers. It is shown that the percolation theory is able to explain easily not only the change of carrier type described in this work but also the discrepancy between the experimental results of different authors [1–6]. Two critical temperatures have been made evident by measuring the conductivity of the p-type layers. The first critical temperature $T_{crit} = 573$ K corresponds to the crystallization temperature of the layers while the other one $T_s \approx 473$ K has been attributed to the phase transition (α-$In_2Se_3 \rightarrow \beta$-$In_2Se_3$) of the microcrystallites embedded in the amorphous matrix. These results are in good accordance with optical and DTA measurements.

Therefore it appears that while usually In_xSe_{100-x} appears to be amorphous when studied with macroscopic techniques, the crystalline state of the layers has to be checked very accurately before any electrical characterization is performed, to avoid erroneous conclusions being reached regarding the change of the type of the majority carriers in these binary amorphous chalcogenides.

References

[1] Ando K and Katsui A 1981 *Thin Solid Films* **76** 141
[2] Kenawy M A, El-Shazly A F, Afifi M A, Zayed H A and El-Zahid H A 1991 *Thin Solid Films* **200** 203
[3] Onys'kiv A B, Orishchin Yu M, Savchin U P, Stakhira I M and Fetsyukh I M 1990 *Sov. Phys.–Semicond.* **24** 264
[4] Watanabe I and Yamamoto T 1985 *Japan. J. Appl. Phys.* **24** 1282
[5] Naito H, Okuda M, Matsushita T and Nakau T 1980 *Japan. J. Appl. Phys.* **19** L513
[6] Ramchandar Rao S, Nagabhooshanam M and Hari Babu V 1990 *Cryst. Res. Technol.* **25** 55
[7] Matsushita T, Nang T T, Okuda M, Suzuki A and Yokota S 1976 *Japan. J. Appl. Phys.* **15** 901
[8] Mott N F and Davis E A 1979 *Electronic Processes in Non-crystalline Materials* 2nd edn (Oxford: Clarendon)
[9] Tohge N, Minani T, Yamamoto Y and Tanaka M 1980 *J. Appl. Phys.* **51** 1048
[10] Kumar S, Kashyap S C and Chopra K L 1992 *Thin Solid Films* **217** 146
[11] Tichy L, Ticha H and Triska A 1985 *Solid State Commun* **53** 399
[12] Marsillac S, Bernède J C and Conan A 1995 *J. Mater. Sci.* 581
[13] Segura A, Guesdon J P, Besson J M and Chevy A 1983 *J. Appl. Phys.* **54** 876
[14] Bidjin D, Popovic S and Celustka B 1971 *Phys. Status Solidi* a **6** 295
[15] Atakishiev S M and Akhundor G A 1969 *Phys. Status Solidi* **32** 33
[16] Chevy A, Kuhn A and Martin S 1977 *J. Cryst. Growth* **38** 118
[17] De Blasi C, Micocci G and Rizzo A 1983 *Phys. Rev.* B **27** 2429
[18] Biswas S K, Chaudhuri S and Choudhury A 1988 *Phys. Status Solidi* a **105** 467
[19] Krishna Sastry D V and Jayarama Reddy P 1983 *Thin Solid Films* **105** 139
[20] Shigetomi J, Ohkubo H and Ikari T 1991 *Thin Solid Films* **199** 215
[21] Clark A H 1983 *Thin Solid Films* **108** 285
[22] Hogg J H C, Sutherland H H and Williams D J 1973 *Acta Crystallogr.* B **29** 1590
[23] Watanabe Y, Kaneko S, Kawazoe H and Yamane M 1989 *Phys. Rev.* B **40** 3133
[24] Rousina R, Shivakumar G K and Yousefi G H 1990 *Vacuum* **41** 1451
[25] Miccoci G, Tepore A, Rella R and Siciliano P 1995 *Phys. Status Solidi* a **148** 431
[26] Nassary M M, Nagat A T and Hussein S A 1994 *Cryst. Res. Technol.* **29** 281
[27] Van Landuyt J, Van Tendeloo G and Amelinckx S 1975 *Phys. Status Solidi* a **30** 299
[28] Likforman A and Carre D 1978 *Acta Crystallogr.* B **34** 1
[29] Popovic S, Celutska B and Bidjin A 1971 *Phys. Status Solidi* a **6** 301
[30] Eddrief M 1984 *Thesis* Paris University
[31] Julien C, Eddrief M, Kambas K and Balkanski M 1986 *Thin Solid Films* **137** 27
[32] Celustka B, Bidjin D and Popovic S 1971 *Phys. Status Solidi* a **6** 699
[33] Werner J H 1984 Origin of curved Arrhenius plot for the conductivity of polycrystalline semiconductors *Polycrystalline Semiconductors III (Physics and Technology of Solid State Phenomena XXX)* ed H P Strunk, J H Werner, B Fortin and O Bonnaud (Zurich: Trans. Tech.)
[34] Tada K, Tanino N, Murai T, Liang Y C and Furutani K 1983 *Thin Solid Films* **108** 293